R-08-27

Analysis of geohydrological data for design of KBS-3H repository layout

Pirjo Hellä, Henry Ahokas, Jorma Palmén, Eveliina Tammisto
JP-Fintact Oy

July 2008

Svensk Kärnbränslehantering AB
Swedish Nuclear Fuel
and Waste Management Co
Box 250, SE-101 24 Stockholm
Tel +46 8 459 84 00

SKB

ISSN 1402-3091
SKB Rapport R-08-27

Analysis of geohydrological data for design of KBS-3H repository layout

Pirjo Hellä, Henry Ahokas, Jorma Palmén, Eveliina Tammisto
JP-Fintact Oy

July 2008

Keywords: Groundwater, Transmissivity, Inflow, Fracture, Disposal of spent nuclear fuel, KBS-3H.

This report is a result of a joint project between SKB and Posiva. This report is also printed as a Posiva WR report, Posiva WR 2006-16.

A pdf version of this document can be downloaded from www.skb.se.

Preface

This work has been done under contract (ORDER 756/401) by Saanio and Riekkola Oy. The contact person has been Margit Snellman, Saanio and Riekkola and Pirjo Hellä and Pauli Saksa at JP-Fintact. Jorma Palmén, Eveliina Tammisto, Eero Heikkinen and Henry Ahokas have prepared the integrated hydraulic conductivity and orientation data for the analysis carried out by Pirjo Hellä. The report has been written by Pirjo Hellä and Jorma Palmén has helped considerably in editing the text and providing figures. Henry Ahokas has provided suggestions and comments extremely helpful during the work. The authors wish to thank Bill Lanyon from Fracture Systems Ltd and Jorma Autio and Margit Snellman from Saanio and Riekkola for their comments on the report.

Abstract

SKB and Posiva are performing an R and D program to develop the KBS-3H repository concept. This work has been done within the Safety Case subproject of the KBS-3H project. The study presents basic information about the occurrence, frequency and orientation of transmissive fractures in the depth interval –300 to –700 m below sea level at the Olkiluoto Island.

The study is based on the observations of transmissive fractures in the boreholes. The major fracture zones and the surrounding rock have been excluded as the aim has been to analyse likely conditions in the deposition drifts. The transmissivity of the fractures ranges from 10^{-10} m^2/s to 10^{-5} m^2/s corresponding to drift inflow of 0.004 l/min and 400 l/min respectively. The overall frequency of transmissive fractures is 4 fractures per 100 m. Especially fractures with transmissivity over $T > 10^{-8}$ m^2/s occur mainly in connection of zones with abundant fracturing. Transmissive fractures tend to form clusters even outside the zones and intervals over hundred metres with no transmissive fractures occur. Drift inflow for 5 m/10 m intervals was estimated based on borehole data. The inflow was less than 0.1 l/min in 90% respectively 85% of the intervals.

There are significant uncertainties in applying the presented results based on the observations from mainly subvertical boreholes to horizontal drifts. In addition to the orientation bias, heterogeneity of the flow within the fractures, connectivity between hydraulic features, effects of grouting and skin effects around the drift will have an effect on the eventual inflows to the deposition drift.

Contents

1 Introduction

SKB and Posiva are performing an R and D program with the overall aim at developing the KBS-3H concept as an alternative to KBS-3V design. A Basic Design Phase was run in 2003. The new KBS-3H phase running from 2004–2007 is divided in Technical development, Demonstration and Safety Case subprojects. This work has been done within the Safety Case subproject.

According to KBS-3H concept the canisters are planned to be deposited in approximately 300 m long horizontal drifts with a diameter of 1.85 m. A canister together with bentonite blocks is placed in a about 5 m long supercontainer. Between the supercontainers distance blocks of bentonite are installed. The combined length of a supercontainer and the adjacent distance block is about 10 m long, see Figure 1-1. The drift will be sealed and plugged soon after the canister emplacement. Inflow of groundwater to the deposition drifts and its interaction with the bentonite buffer are key issues when considering the feasibility and safety of the KBS-3H concept.

The objective of the study is to collect basic information about the occurrence, frequency and orientation of water bearing fractures in the depth interval –300 to –700 m below sea level at the Olkiluoto island. The interest lies in the scale relevant to the deposition drifts of the KBS-3H alternative (~1 – < 100 m) and in transmissive fractures, fracture groups and narrow fracture zones, which may have effect on the design of drifts and repository layout, may require groundwater control actions and are also of importance for the long-term safety of the repository. The study also discusses the occurrence of transmissive fractures relative to the crushed and fracture zones and overall fracture intensity. At the current stage, the other fracture properties like infilling material etc. obtainable from the core sample are not analysed. The basic source of data has been the flow loggings in the boreholes and TV-images of the borehole walls, therefore no estimation of the fracture or zone size has been made. Earlier, the effect of fracturing taking into account orientation, fracture infillings and hydraulic properties on tunnel orientation has been studied by /Rautakorpi et al. 2003/. In addition, specific studies on fracture networks and fracture properties have been presented by /Poteri 2001/ and /LaPointe and Hermansson 2002/. Statistical analysis on the existence of fracture zones has been reported in /Hellä et al. 2004/.

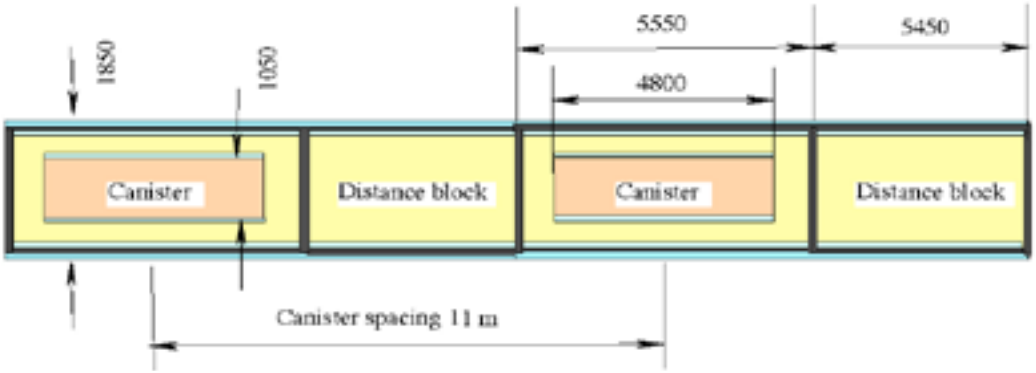

Figure 1-1. *Principle of KBS-3H layout alternative with main dimensions (Figure 1 in /Ikonen 2005/).*

2 Data

2.1 General

In the study, the boreholes which provide information both on fracture transmissivity and orientation in the relevant depth range –100 m to –700 m below sea level are included. The boreholes have an inclination ranging from 50° to 90° and most of them are drilled towards north-northwest (see Figure 2-1 and Table 2-1). The borehole diameter is either 56 mm or 76 mm. The total sample length in the depth range of interest is close to 5,000 m.

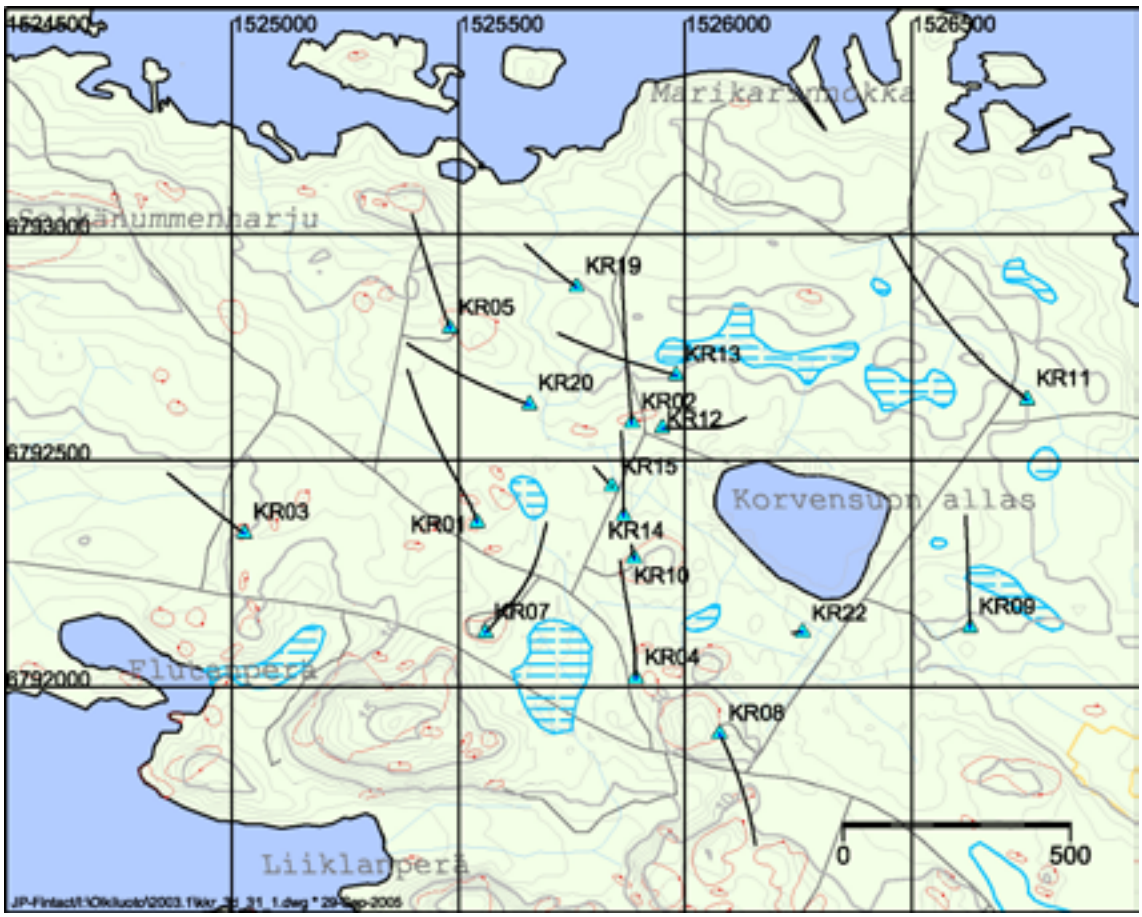

Figure 2-1. *Surface map showing the location boreholes and projection of borehole trajectories.*

Table 2-1. Summary of data included in the study and compiled from the Posiva Working reports referred in the table.

Borehole	Azimuth (degrees)	Inclination (degrees)	End depth (mbsl)	Borehole length range, start (m)	End (m)	Report reference
OL-KR1	341	75	–889.29	325	750	/Rouhiainen 2000/
OL-KR2	359	76	–961.20	325	750	/Rouhiainen 2000/
OL-KR3	306	68	–434.90	325	502	/Rouhiainen 2000/
OL-KR4	0	77	–847.37	325	750	/Rouhiainen 2000/ /Hellä et al. 2004a/
OL-KR5	340	65	–474.28	350	558.85	/Rouhiainen 2000/
OL-KR7	43	70	–632.96	325	811.05	/Pöllänen and Rouhiainen 2001a/ /Hellä et al. 2004a/
OL-KR8	155	64	–529.40	350	600.59	/Rouhiainen 2000/ /Hellä et al. 2004a/
OL-KR9	360	70	–538.36	325	601.25	/Rouhiainen 2000/ /Hellä et al. 2004a/
OL-KR10	0	90	–602.39	300	614.4	/Rouhiainen 2000/ /Hellä et al. 2004a/
OL-KR11	310	70	–869.60	325	800	/Rouhiainen 2000/
OL-KR12	90	70	–749.80	325	725	/Pöllänen and Rouhiainen, 2001a/
OL-KR13	285	56	–408.29	375	500.21	/Pöllänen and Rouhiainen, 2002a/
OL-KR14	0	70	–458.44	325	514.1	/Pöllänen and Rouhiainen, 2002a/
OL-KR15	321	89	–503.48	300	518.85	/Pöllänen and Rouhiainen, 2002c/
OL-KR19	307	76	–516.22	325	544.34	Draft
OL-KR20	290	50	–384.91	400	494.72	Draft
OL-KR22	271	59	–389.34	350	500.47	Draft

2.2 Transmissivity

The transmissivity of fractures in the boreholes has been measured using the difference flow meter (Figure 2-2). The difference flow meter measures flow from fractures into a borehole or out from a borehole into bedrock within the test section. The flow is measured both without pumping and by pumping the borehole with a submersible pump at shallow depth in the borehole. During the measurement, there is no pressure difference between the test section and the rest of the borehole which makes the use of flexible rubber disks instead of inflatable packers possible /Öhberg and Rouhiainen 2000/. Mainly the results from a logging in detailed mode are used here (see Table 2-1 for references). In the detailed mode measurement, the tool is moved with steps shorter than the length of the test section itself. Typical depth increments have been 0.1 m with a 0.5 m test section. This enables the measurement of fracture specific flow, as the short depth interval makes it possible to determine the exact depth of the flow point (fracture) and the flow from or into a certain fracture is measured several times during the logging procedure. In the detailed mode, the flow is measured using the thermal dilution method. The theoretical detection limit of thermal dilution method is 0.5 ml/min, but in practice the limit can be higher, depending on the composition of the groundwater. When converting the measured flow into transmissivity this means that in practice transmissivities below $10^{-9.5}$ m^2/s cannot be systematically measured. Figure 2-3 gives an example of the results.

In addition, results from constant head injection tests with double-packers using the Hydraulic Testing Unit (HTU) /Hämäläinen 1991ab, 1997a–e/ and from difference flow meter measurements in normal mode /Pöllänen and Rouhiainen 1996ab, 2000, 2001, 2002a–d/, and /Rouhiainen 2000/ have been used in checking results. These techniques give the total flow

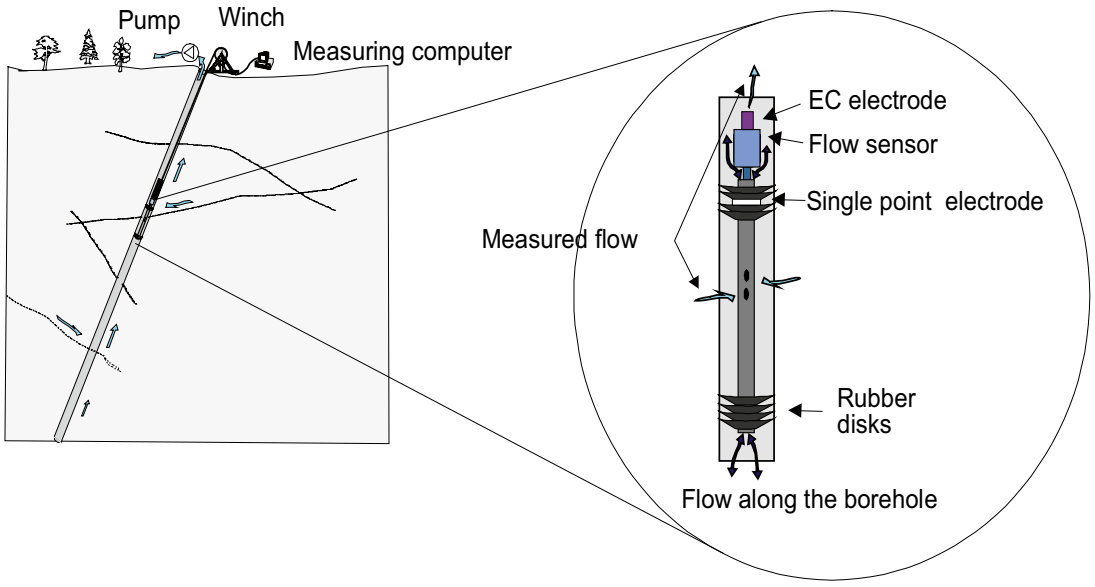

Figure 2-2. *The difference flow meter down-borehole tool (figure from /Öhberg and Rouhiainen 2000/). The downhole tool (electronic tube above the flow sensor not presented) and flow directions are shown for the situation when pressure in the borehole is lower than in the bedrock i.e. inflow into the borehole. The water from fractures flows through the flow and electrical conductivity (EC) sensors (light blue arrow). The flow of borehole water along borehole (dark blue arrow) is directed through the tool via the bypass tube.*

of the test section having typically length of 2m, although in the earlier HTU-measurements test intervals could be as long as 31 m.

A rough estimate of the inflow to the drift (Q, l/min) can be calculated from the fracture specific transmissivity (T, m^2/s) according to Thiem's equation (Equation 1) assuming steady state radial flow with constant head. The radius of influence (r_0) is assumed to be 50 m and the head Δh 420 m i.e. equivalent to the repository depth. In Equation 1, r_t marks the radius of the deposition drift (0.925 m).

$$Q = \frac{2\pi\Delta hT}{\ln(r_0/r_t)}$$

Equation 2-1

Later in this study the fractures observed to be hydraulically conductive are called transmissive fractures. The analysis is based on the transmissivity and spacing of the fractures. For the reference, the inflow to the deposition drift equivalent to the fracture specific T values and calculated according to Equation 1 is also presented. An estimate of the drift inflow per 5 m and 10 m intervals (Q_{5m} and Q_{10m} (l/min)) is calculated by summing the transmissivities of respective borehole intervals and converting the transmissivity to the equivalent inflow to the drift using Equation 1.

2.3 Fracture data

Information on orientation of the transmissive fractures can be used in the design of the repository. The design can be optimized e.g. with respect to inflow positions, total inflow or distribution of inflows depending on the available data.

Fracture orientation data used in this study is obtained from the borehole optical imaging. At Olkiluoto, three different optical imaging techniques have been applied (BIP, OPTV and OBI40, for references see Table 2-1). The images consist of bitmaps arranged by depth and

by orientation, see Figure 2-3 for an example. Images have been acquired by slowly lowering a wire-line probe into the borehole. In the probe the light from a source is reflected from borehole wall to a mirror or a prism, from where it is further projected onto CCD-element or a digital camera. The pixel resolution of the resulting image has varied (0.2–1 mm) depending on the applied technique and logging speed. The physical resolution of the system is 0.5 mm, but the aperture of continuous fractures can be determined with even greater accuracy by analyzing the subpixel information from neighboring pixels. During the logging, the tool orientation relative to the borehole is measured; this can then be combined with the other borehole orientation data to align the image relative to site north.

From the image it is possible to map and orient fractures which can then be integrated with other borehole data provided the depth is properly adjusted. Combined conductivity and orientation data determined from the image was readily available for boreholes OL-KR4, OL-KR7–OL-KR10 /Hellä et al. 2004a/. Otherwise the orientation of transmissive fractures was determined from the images in the earlier phase of this study. Fracture mapping was done by importing the images into WellCAD program /ALT 2001/. Also, in combining the image orientation and conductivity data WellCAD software was used.

2.4 Classification of data

Prior to the analysis, the transmissive fracture data was classified based on whether it belongs to fracture or crushed zones known to have larger extension, to smaller zones or outside the zones. The classification is based on the current version of the Olkiluoto bedrock model (v. 2003/1, /Vaittinen et al. 2003/). In the bedrock model borehole sections, which have fracture frequency over 10 fractures/m on at least 2 m borehole interval or are classified to belong to classes Ri IV or Ri V according to the engineering geological mapping /Korhonen et al. 1974, Gardemeister et al. 1976/, are modeled as either crushed and fracture zones. Additionally intervals with high hydraulic conductivity ($K_{2m} > 5 \cdot 10^{-7}$ m/s) are modeled as hydraulic features.

The transmissive fractures within crushed or fracture zones RH9, RH20A, RH20B, RH20C and RH21 (called later major fracture zones) and close to them (20 m margin) have been excluded from the analysis. The location of the zones is presented in Figure 2-4. These zones have been observed to have larger extension and are also hydraulically conductive. The location of deposition drifts is assumed to be at depth of –420 m, which is mainly below the zone RH20 (including parts A, B and C). This zone is subhorizontal dipping towards southeast and hydraulically highly transmissive (T in the order of 10^{-5} m^2/s). Below this zone hydraulic conductivities are small with very few exceptions as can be seen in Figure 2-5, showing all transmissivities higher than 10^{-7} m^2/s. Deeper in the bedrock some transmissive sections exist and they belong mainly to the zone RH21, which is also dipping gently towards southeast. Figure 2-5 points out how the rock is clearly more hydraulically conductive close to the surface as in the depth range considered here.

The major fracture zones are to be avoided and considered to be known before excavating deposition drifts and are therefore not of interest in analyzing the rock properties typical in the deposition drifts. Still, these zones are taken into account when calculating the distances from transmissive fractures to crushed or fracture zones and also in counting the distances between transmissive fractures. The analysis still includes transmissive fractures and intervals within other crushed or fracture zones (called later local or just fracture zones and shown in Figure 2-4) and as well as outside the zones. Statistics are calculated for all of the fractures and separately for fractures within the local zones and outside them. The sample length included in the study after removing the major fracture zones and their margin is roughly 4,000 m.

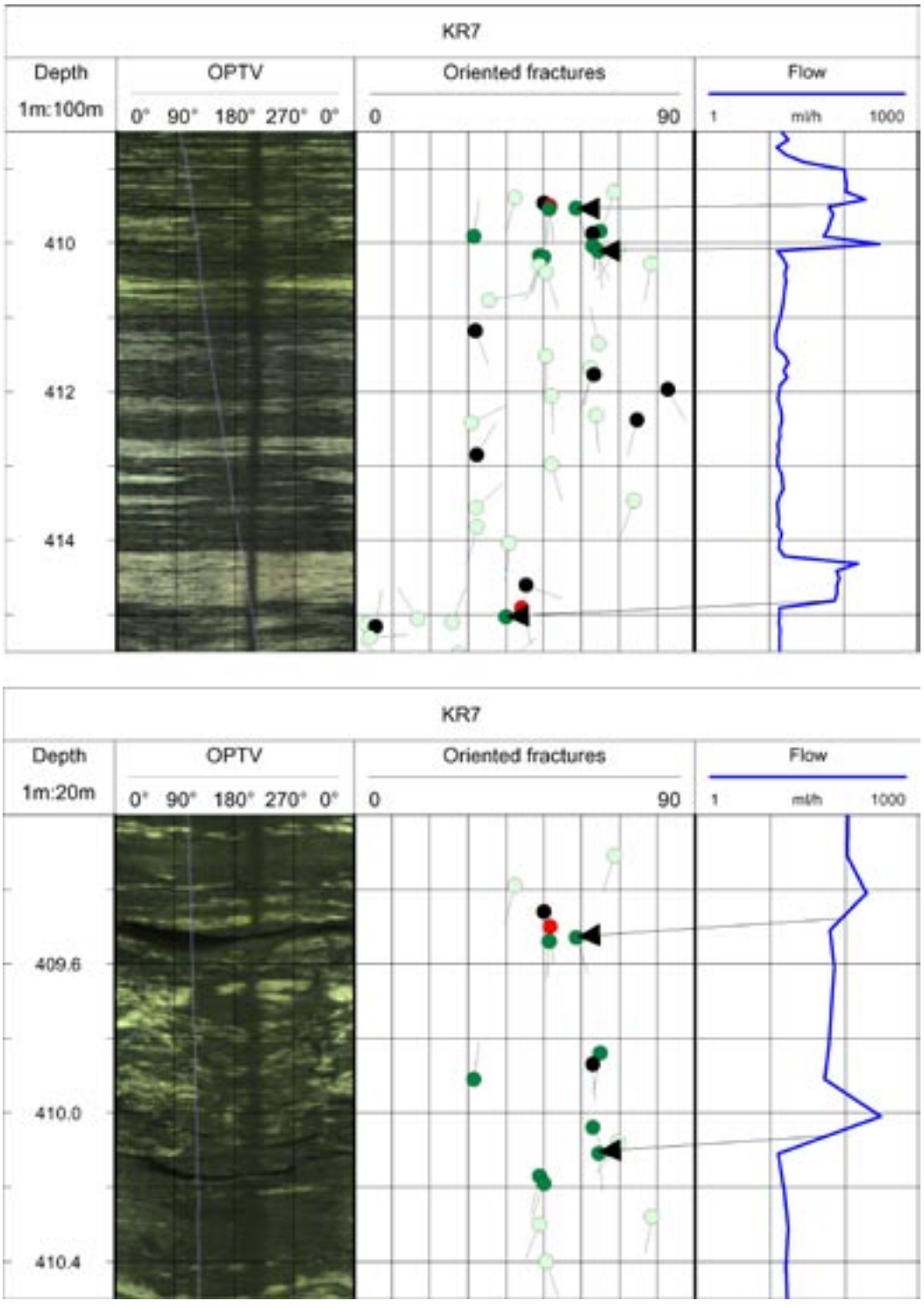

Figure 2-3. *Example of the borehole wall image (on the left), fracture data (in the middle) and hydraulic conductivity (flow) measured using difference flow meter in detailed mode (on the right). The lower figure shows a detail from the upper figure. Correlation of the recognised hydraulic features to fractures is shown by the arrows. The example is from borehole OL-KR7. In the image the light line shows the tool orientation in the borehole, the dark vertical line is due to the material accumulated on the down side of the borehole. The grid is aligned to North, East, South and West respectively.*

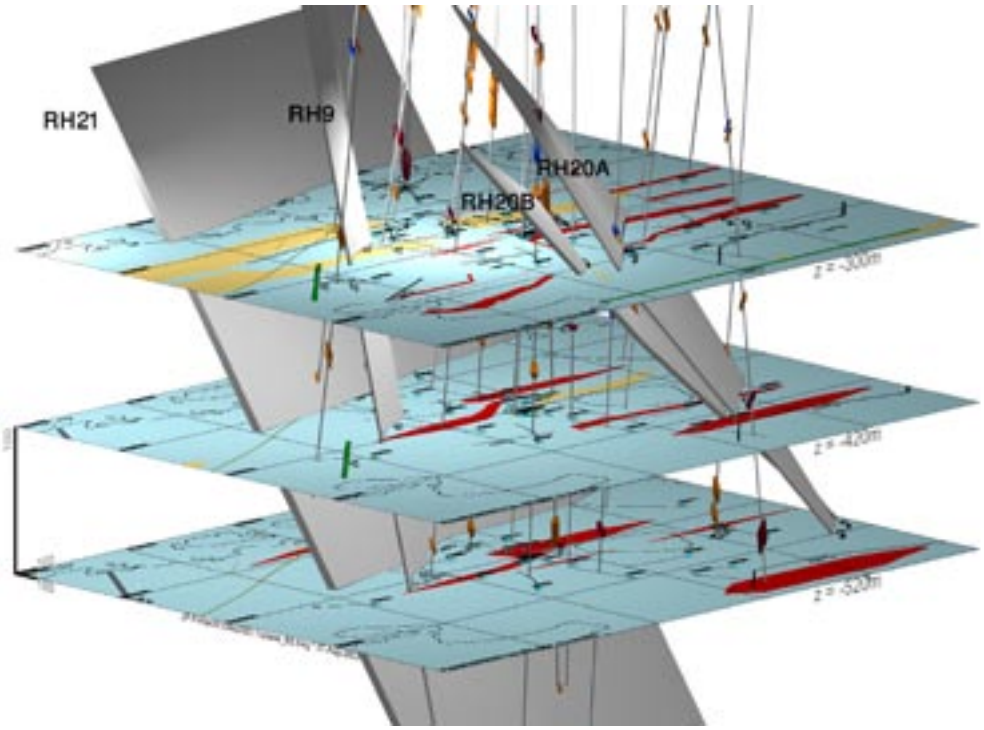

Figure 2-4. *The horizontal cross-sections of the bedrock model are located at the depths of –300 m, –420 m, and –520 m. Structures RH9 (in the middle), RH20A, RH20B(on the right) and RH21(at back) – the ones excluded from the analysis – are shown as 3D objects. Structure intersections with boreholes are shown along boreholes. The vertical scale is five times to the horizontal scale. Figure from /Vaittinen et al. 2003/.*

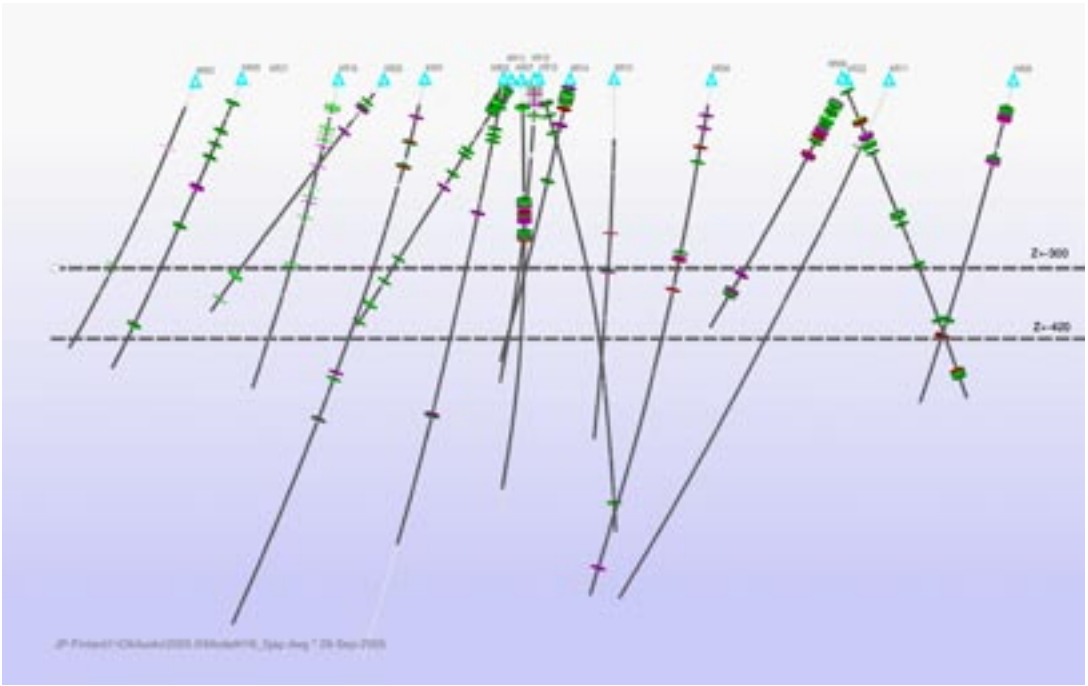

Figure 2-5. *Transmissivities (T_{2m}) higher than 10^{-7} m^2/s classified with colors into three sets (red $T > 1 \cdot 10^{-5}$, purple $1 \cdot 10^{-5} > T > 1 \cdot 10^{-6}$, green $1 \cdot 10^{-6} > T > 10^{-7}$) in boreholes used in the analysis of this report. The upper dotted line is placed at depth of –300 m, upper limit of the depth range included in this study). The lower line presents the repository depth of –420 m. View is towards northeast.*

3 Characteristics of the transmissive fractures

3.1 Transmissivity

The observed transmissivity of the fractures ranges from 10^{-10} m^2/s to 10^{-5} m^2/s corresponding to drift inflow of 0.004 l/min and 400 l/min respectively. Table 3-1 presents the basic statistics of the transmissivity (log) values observed in the depth range –300 to –700 m outside the major fracture zones. In Figure 3-1 both the frequency and cumulative distribution of the transmissivity (log) of the fractures is presented. As can be seen from the Figure 2-1 and deduced from the data in Table 2-1, conductive fractures occur both within and outside zones, but the fractures with higher transmissivity occur mainly within fracture zones. The transmissivity seems to be log normally distributed. The observed median transmissivity outside zones $10^{-8.8}$ m^2/s equals to drift inflow of 0.07 l/min and median transmissivity within zones $10^{-8.0}$ m^2/s is equivalent to drift inflow of 0.4 ml/min.

3.2 Frequency of transmissive fractures

The spacing of transmissive fractures (all fractures with observed conductivity, $T > 10^{-10} – 10^{-9.5}$ m^2/s) i.e. distance between two adjacent fractures along borehole is presented in Figure 3-2 and the basic statistics in Table 3-2. The transmissive fractures seem to occur rather close to each other as the mean distance is around 6 m. On the other hand, there are also intervals over 100 m with no transmissive fractures – such intervals comprise roughly one fifth of the total sample length. The distance between transmissive fractures follows approximately the lognormal distribution.

The clustering of transmissive fractures becomes more evident if the minimum distance from a transmissive fracture to the next transmissive fracture is considered rather the spacing between transmissive fractures. Figure 3-3 shows the correlation between transmissivity of the fracture and the distance from the fracture to the next (closest) transmissive fracture. In calculation of the minimum distance all fractures with measurable flow are considered regardless of the conductivity. In Figure 3-4 the distribution of the minimum distance is presented. Proportion of fractures lying further than 10 m apart from another transmissive fracture is only 15%.

Table 3-1. Basic statistics of the transmissivity (log(T (m²/s) values of the fractures. In the table also an estimation of the corresponding inflow (Q (l/min)) according to Equation 1 is given.

	All (logT)	All (Q)	Within fracture zones (logT)	Within fracture zones (Q)	Outside fracture zones (logT)	Outside fracture zones (Q)
Count	175	175	57	57	118	118
Min	–10.0	0.004	–9.5	0.01	–10.0	0.004
Max	–5.0	356.9	–5.0	356.9	–6.2	27.0
Median	–8.6	0.1	–8.0	0.4	–8.8	0.1
Average	–8.4	3.4	–7.9	8.7	–8.6	0.9
Stdev	0.9	27.2	1.0	47.2	0.8	3.6
I quartile	–9.1	0.03	–8.7	0.1	–9.2	0.03
III quartile	–7.9	0.5	–7.3	2.0	–8.1	0.3

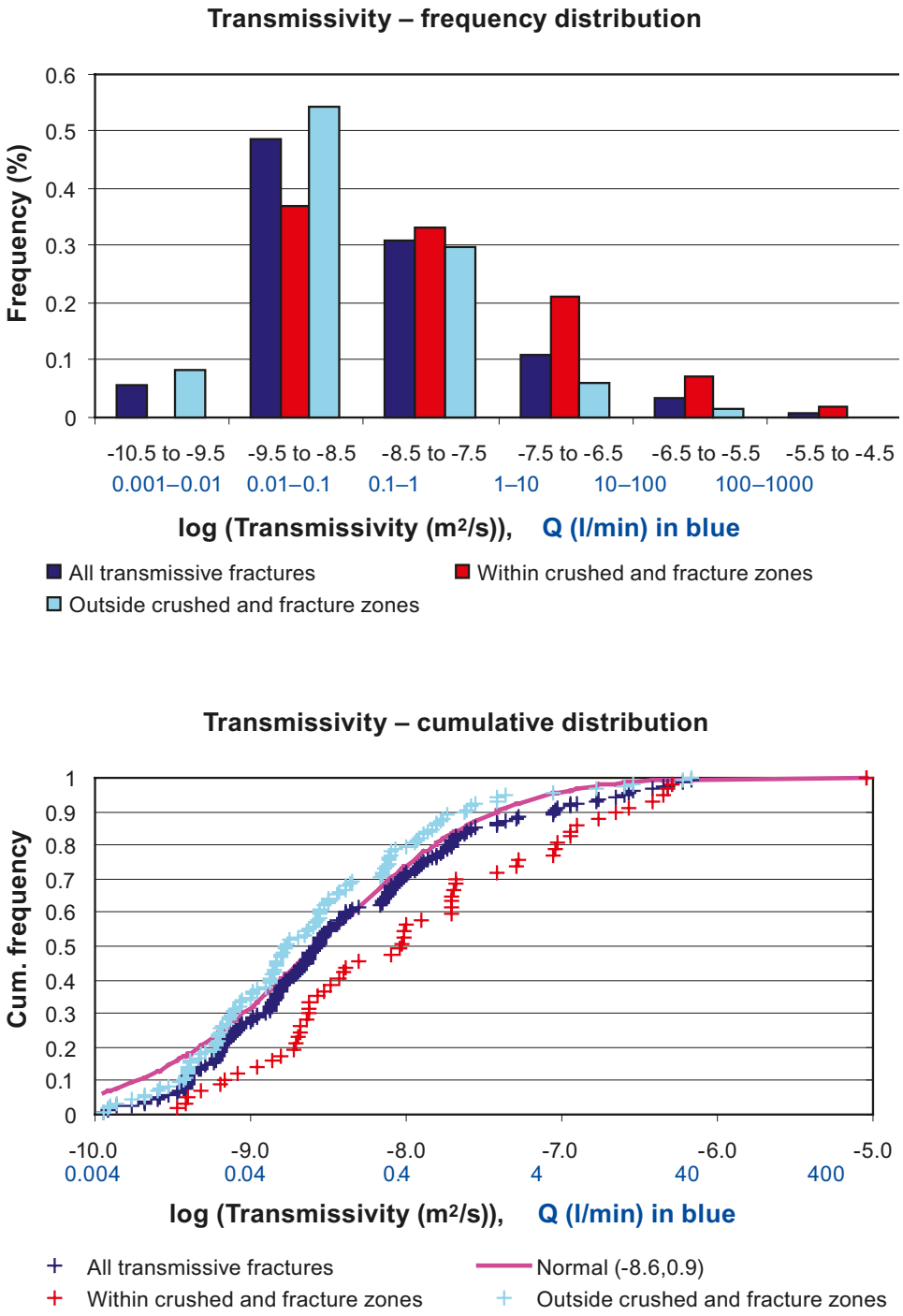

Figure 3-1. *Transmissivity of fractures; frequency distribution (top) and cumulative distribution (lower figure). For the reference also the estimated inflow to the drift according to Equation 1 is presented.*

Table 3-2. Basic statistics of the distances (m) between hydraulically conductive fractures in two cases; all transmissive fractures considered and only fractures with transmissivity higher than 10^{-8} m^2/s considered.

	All transmissive fractures	Fractures with $T > 10^{-8} m^2/s$
Count	180	87
Min	0.003	0.01
Max	193.37	505.20
Median	6.12	26.13
Average	19.67	65.24
Stdev	32.47	100.44
I quartile	1.44	3.78
III quartile	23.30	70.49

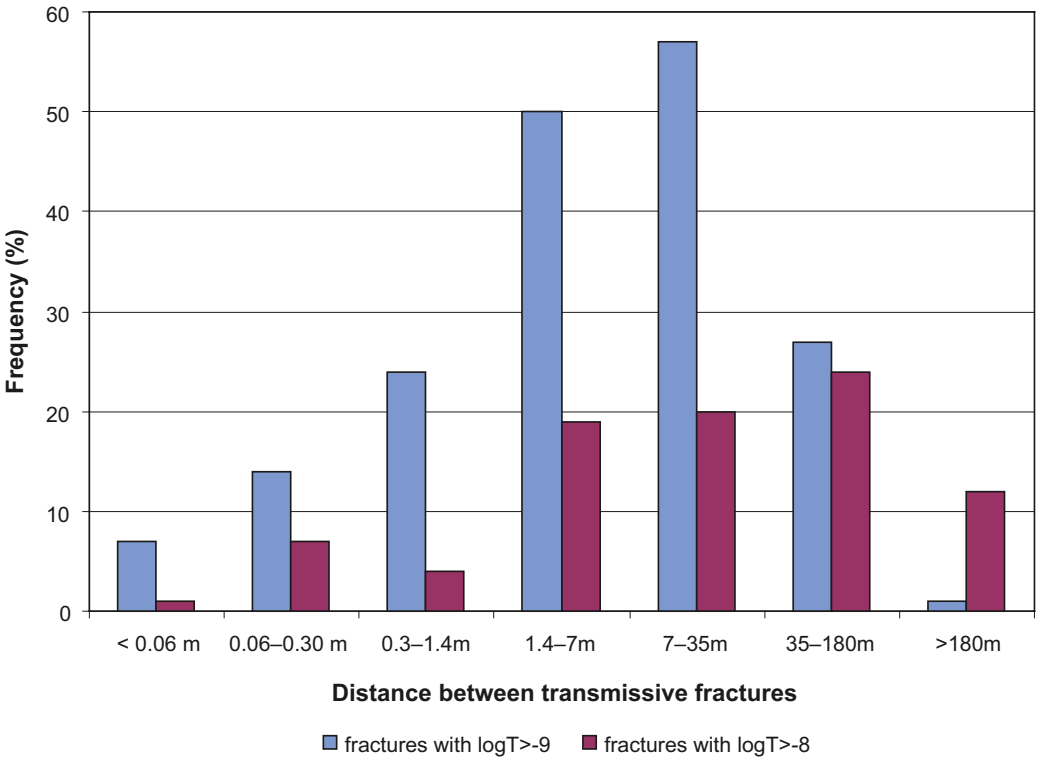

Figure 3-2. *Distribution of the spacing between transmissive features along borehole, in lilac fractures with $T > 10^{-9}$ m^2/s, in plum distances between transmissive fractures with $T > 10^{-8}$ m^2/s ($logT > -8$). In the figure, the spacing is divided in categories for which the logarithm of spacing is equal.*

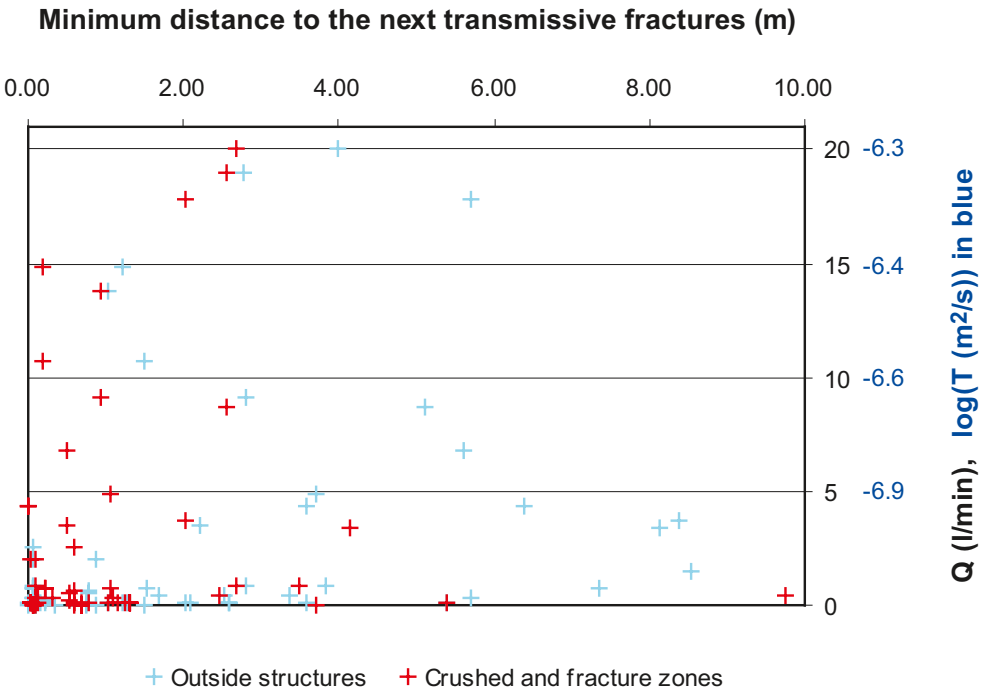

Figure 3-3. Correlation between transmissivity of a fracture (and corresponding inflow Q to the drift) and distance to the closest transmissive fracture, the fractures within local zones are marked with red and fractures outside local zones in turquoise.

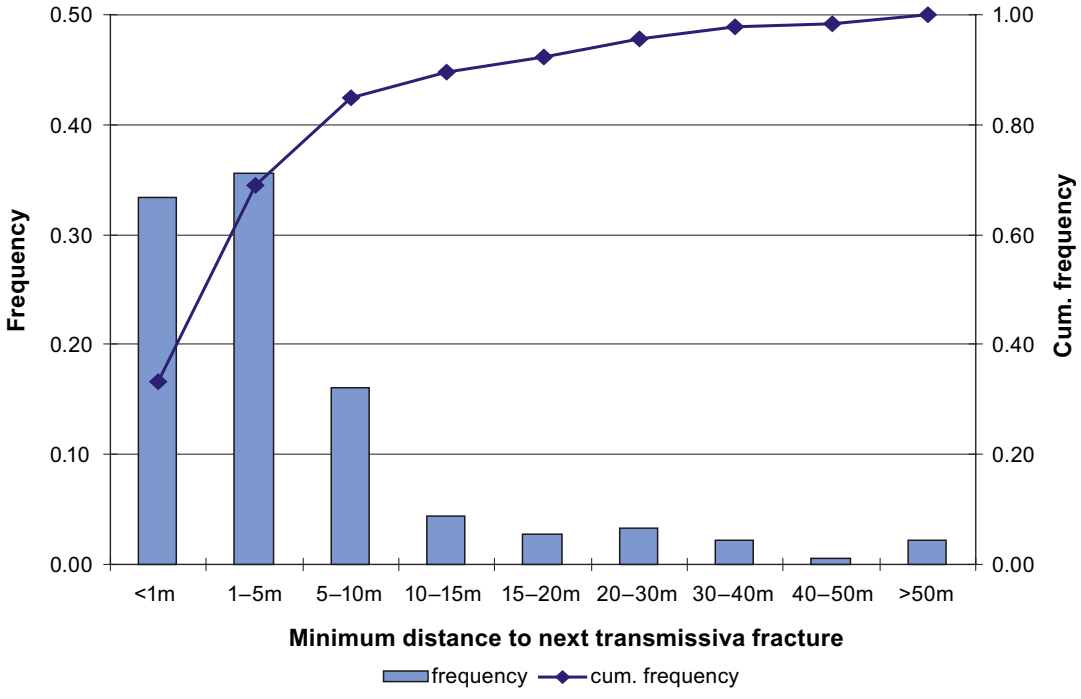

Figure 3-4. Distribution of the minimum distance to the next closest transmissive fracture, all transmissive fractures with measurable flow included.

Even though there is variation in data, the higher transmissivities are mostly observed in fractures close to other transmissive fractures. This is true for transmissive fractures both within and outside fracture zones. Still, there are a couple distinct transmissive fractures even with transmissivity over 10^{-8} m^2/s (corresponding to 0.4 l/min drift inflow) with no other transmissive fracture within tens of meters.

Additionally, the spacing between transmissive fractures was counted for different limiting transmissivities. In the analysis fractures having a transmissivity less than the limit were omitted and the spacing between the remaining fractures were counted. In calculating the distances, the spacing between a fracture and either the major zone boundary (see chapter 2.4) or the further-most transmissive fracture within the excluded margin of the zone were taken into account. The intervals between transmissive fractures within the major zones or their margins were excluded. Also the nearest transmissive fracture outside the studied depth interval was taken into account in calculating the spacing. The results are shown in Figure 3-5. The figure shows the tendency to longer intervals between transmissive fractures with the increasing transmissivity limit. When all transmissive fractures are considered, the median spacing is about 6 m, for fractures with T higher than $10^{-9.5}$ m^2/s (equivalent to drift inflow of 0.01 l/min) the median is approximately 20 m and for fractures with T higher than 10^{-8} m^2/s (equivalent to drift inflow of 0.4 l/min) the median is approximately 30 m. Correspondingly the proportion on long intervals between transmissive fractures increases. For example, intervals over 100 m with no transmissive fractures form about one fifth of the sample length, but in case of fractures with transmissivity higher than $10^{-9.5}$ m^2/s (equivalent to drift inflow of 0.01 l/min) the proportion of such long intervals is already close to 50% of the total sample length and in case of fractures with transmissivity higher than 10^{-8} m^2/s (corresponding to drift inflow of 0.4 l/min) such long intervals cover roughly 80% of the sample length. For example in borehole OL-KR7, no fractures with transmissivity higher than 10^{-8} m^2/s exists, not even within major zones.

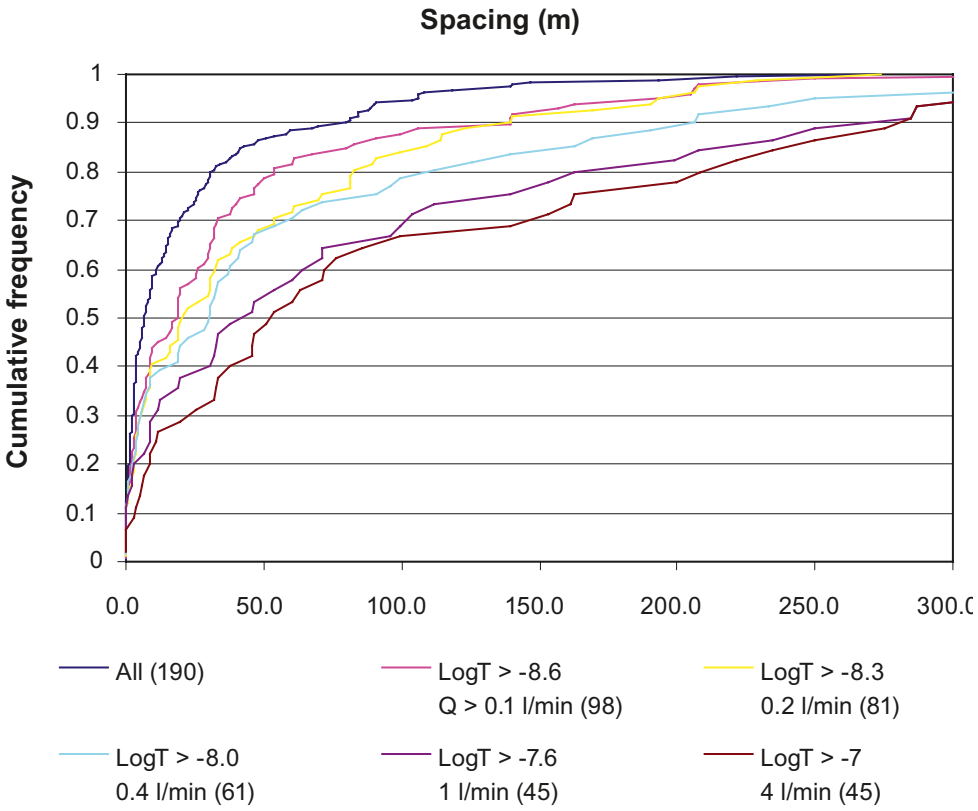

Figure 3-5. *Cumulative distribution of the spacing between transmissive features along borehole for different limiting transmissivity values. Note the figure shows the distribution of the spacing and is not scaled with the sample length.*

3.3 Fracturing around transmissive fractures

Fracture frequency

Figure 3-6 presents the transmissivity and corresponding drift inflow according to Equation 1 as a function of the number of fractures around the transmissive fracture. Higher transmissivity also outside the zones is related to abundant fracturing, although occasionally, transmissivities over 10^{-7} m^2/s occur also in sections with less than 5 fractures per meter, but then there are other transmissive fractures nearby, see also Figures 3-3 and 3-4.

Effect of Fracture zones

Roughly one third of the transmissive fractures occur within local zones (see Table 3-2 and Figure 3-7). In boreholes, the frequency of the local zones is approximately one per 150 m. The transmissivity of fractures outside the local zones as function of the distance to the closest zone is presented in Figure 3-7. There are signs that the transmissivity decreases with an increased distance from a zone. The number of transmissive fractures within few meters from the zones is very small and no high transmissivities are observed. This is due to the definition of zones in the bedrock model, as the two meter sections with high conductivities adjacent to fractured sections are included in the interpreted zone. The observations of fractures having transmissivity over $10^{-7.5}$ m^2/s and a distance to a zone over 10 m were checked case by case. Most of these observations come from the upper part studied depth interval i.e. fractures are located close to –300 m level. Two of theoutliers are from borehole OL-KR13 at length of about 490 m, where there fracture frequency is increased (over 10 fractures per meter) over a short interval.

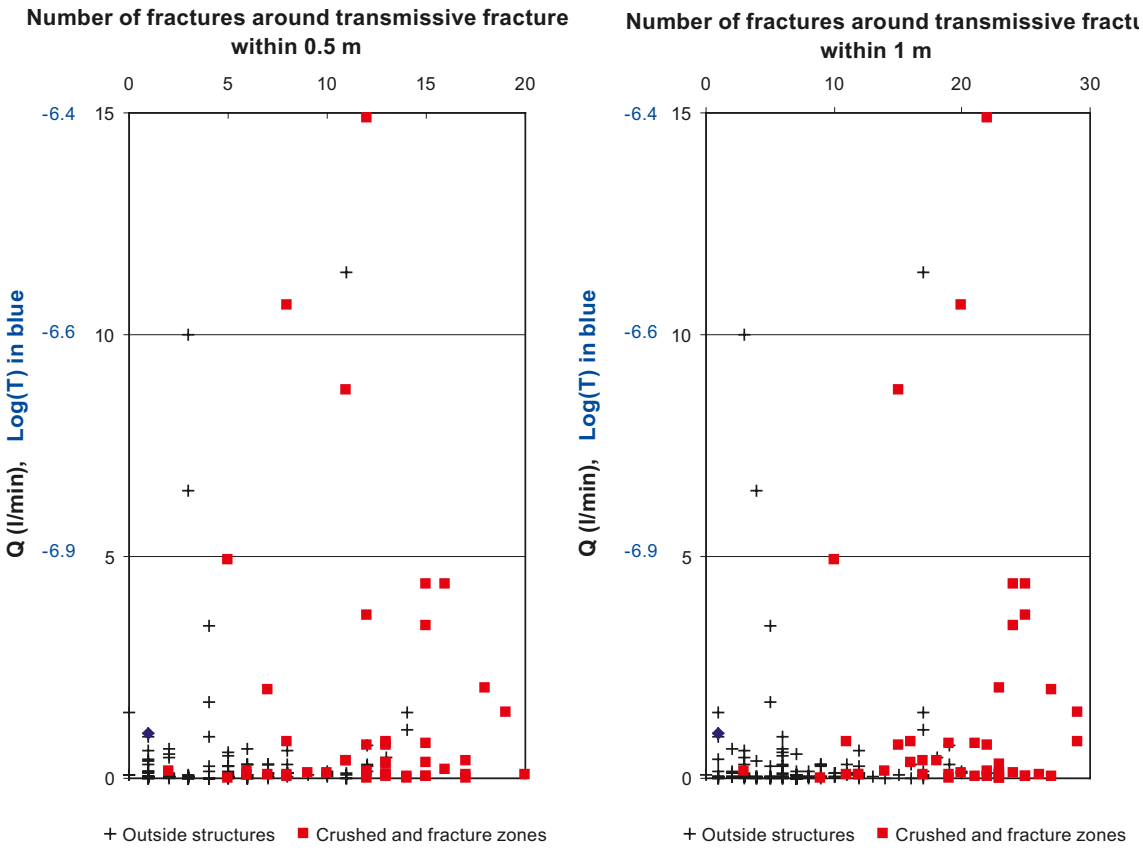

Figure 3-6. *Transmissivity as a function of the number of fractures around the water bearing fracture; on the left within ±0.5 m from the fracture and on the right within ±1 m from the fracture.*

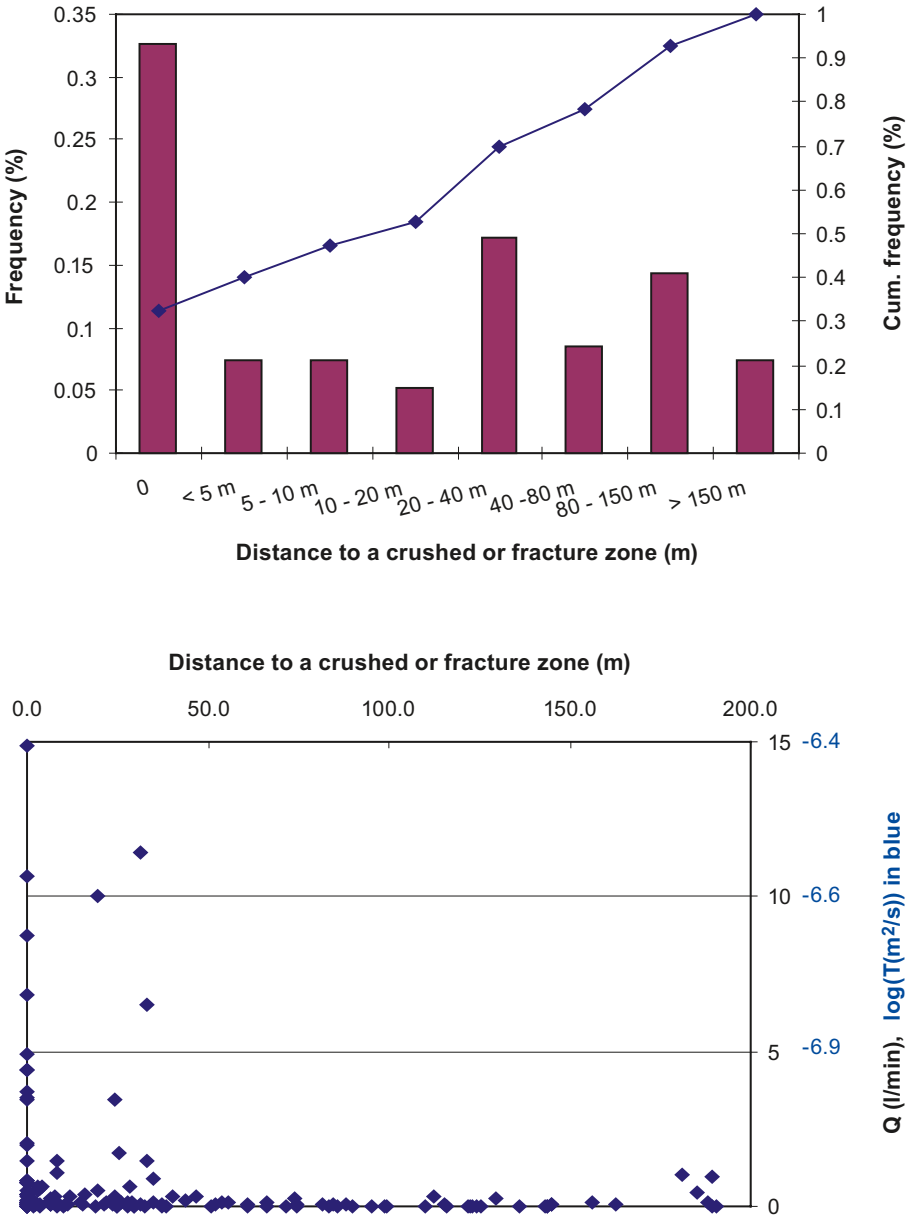

Figure 3-7. *Transmissivity as a function of distance to a fracture zone. Fractures within the zones are included in the first category, for which the distance to fracture zones is 0 m.*

Based on the analysis presented above, the data set was classified according to the distance to the zones. A bit arbitrary limit distance 35 m from the zone was selected based on Figure 3-7, so that all high transmissivities fall in the class < 35 m from the zone. The fractures within the zones form their own group. As a result the data set is divided to three groups with roughly equal number of fractures in each. Further on, the data was classified also according to the transmissivity value (in parenthesis the corresponding drift inflow according to Equation 1):

1. Fractures with $T > 10^{-7}$ m²/s (corresponds to flow > 4 l/min).
2. Fractures with 10^{-8} m²/s < $T < 10^{-7}$ m²/s (corresponds to flow in range 0.4 l/min–4 l/min).
3. Fractures with $T < 10^{-8}$ m²/s (corresponds to flow < 0.4 l/min).

Table 3-3 gives also the frequency as transmissive fractures per borehole length (1/m). On average there are four transmissive fractures per 100 m sample length, but fractures with flow over 4 l/min have a density frequency of only one per 250 m sample length. Fractures with flow between 0.4 l/min and 4 l/min have a frequency of one per 100 m.

Table 3-3. Summary of transmissivity values and their occurrence within local zones, margins of the zones and in averagely fractured bedrock.

Transmissivity T (m^2/s)/ distance to the zone (m)	Within local zones d = 0 m	Margin of the local zone 0 m < d < 35m	Outside local zones d > 35 m	Sum	Fractures/m
T > 10^{-7} m^2/s	11	5	0	16	0.004
10^{-8} m^2/s < T < 10^{-7} m^2/s	17	12	7	36	0.01
T < 10^{-8} m^2/s	29	45	49	123	0.03
Sum	57	62	56	175	0.04
Sample length (appr.)	180	1,520	2,350	4,050	
Fractures/m	0.32	0.04	0.02	0.04	

3.4 Orientation

Orientation of the transmissive fractures in different transmissivity classes and within and outside zones are presented in the Figure 3-8. As the number of transmissive fractures is so small and there is bias in the data caused by subvertical orientation of investigation holes, no definite conclusions of the orientation distribution can be drawn. There seems to be no clear relationship between fracture orientation and transmissivity.

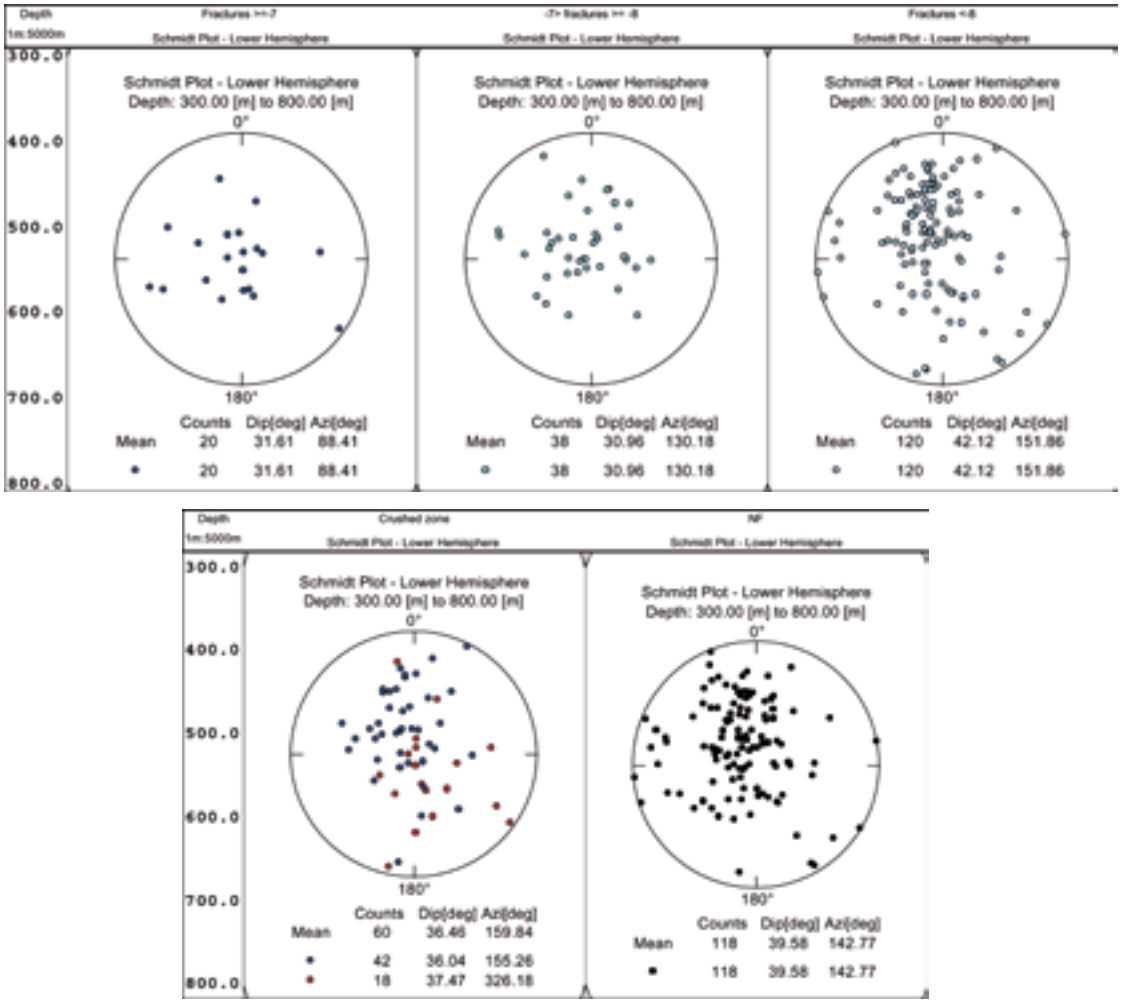

Figure 3-8. *Orientation of the transmissive fractures in the three transmissivity classes (upper) and (lower left) orientation of the transmissive fractures within (red crushed zones, blue fracture zones) local zones and (lower right) outside local zones on an equal area lower hemisphere projection.*

4 Estimation of inflow to deposition drifts

4.1 Inflow to drift on 5 m and 10 m intervals

An estimate of the inflow to the deposition drift per 5 m (Q_{5m}) and 10 m (Q_{10m}) intervals is calculated by summing the fracture transmissivities on respective borehole intervals and calculating the equivalent drift inflow according to Equation 1. The basic statistics of the drift inflow Q_{5m} and Q_{10m} are presented in Table 4-1. Figure 4-1 shows the distribution of Q_{5m} and Q_{10m}. It can be seen that over 90% over the 5 m interval have drift inflow below 0.1 l/min. If the 10 m sections are considered the number of sections with drift inflow below 0.1 l/min is over 80%. This means that there would be likely two 5 m and one or two 10 m intervals per 100 m drift length with inflows higher than 0.1 l/min i.e. around six 5 m and four to five 10 m sections

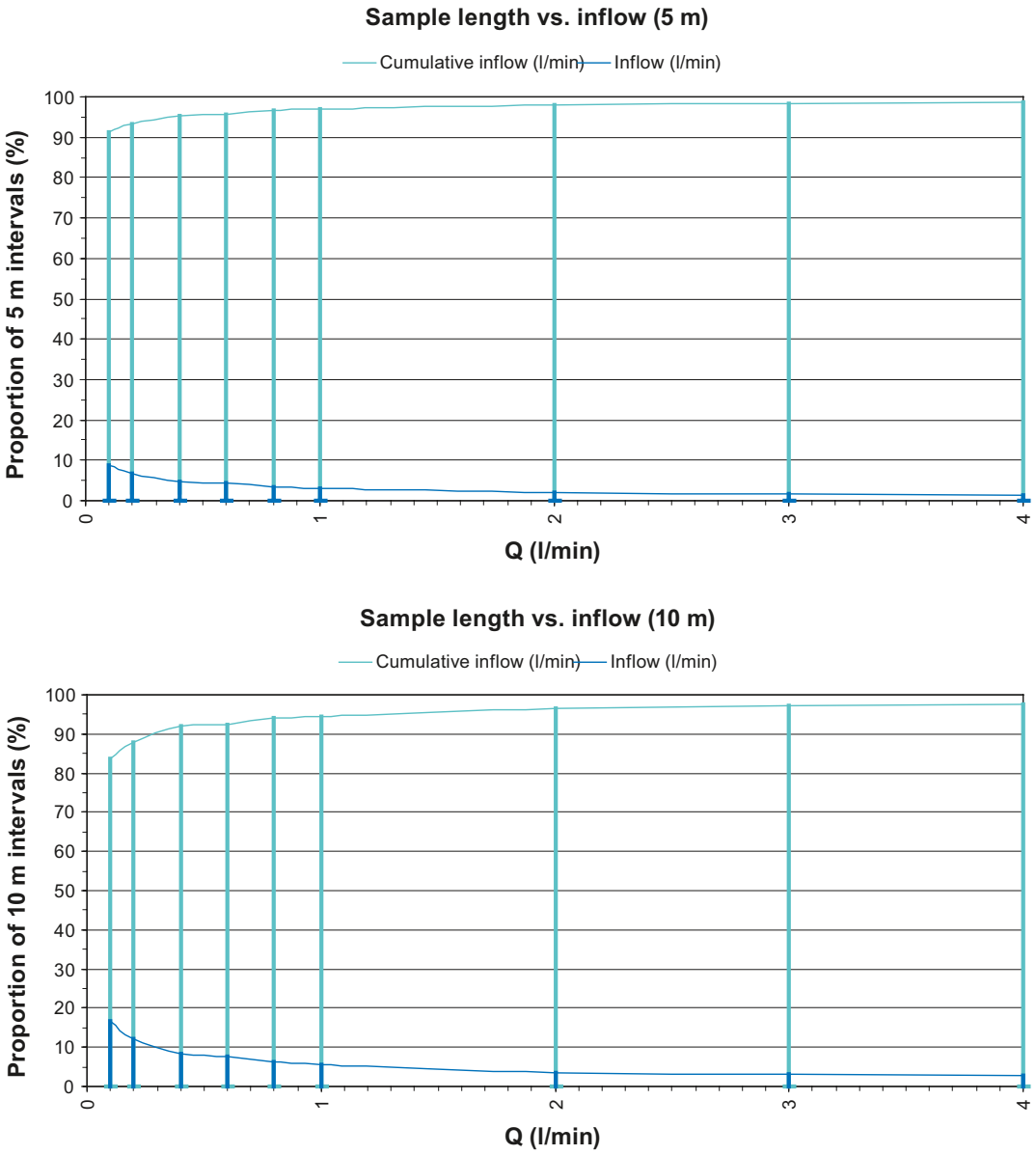

Figure 4-1. *Distribution of the estimated inflow based on 5 m (Q_{5m}) and 10 m (Q_{10m}) borehole intervals. The light blue bars show the cumulative number of intervals being less than the given Q and the dark blue bars show the proportion of intervals having flow greater than the given Q.*

Table 4-1. Basic statistics of the drift inflow on 5 m (Q5m, l/min) and 10 m (Q10 m l/min) intervals.

	Q_{5m} containing local fracture zones	Q_{5m} outside local fracture zones	Q_{10m} containing local fracture zones	$Q_{10\,m}$ outside local fracture zones
Count	28	772	27	373
Min	0.015	0.005	0.015	0.007
Max	357.1	38.4	357.7	38.4

per the planned 300 m deposition drift. This agrees with the estimated number of inflow points, 4 per 100 m, keeping in mind the clustering of the transmissive fractures. The highest observed drift inflow is in both cases about 350 l/min. Table 4-1 shows also clearly the significance of the zones on the estimated drift inflow, both the maximum and median drift inflow are nearly ten times higher on intervals containing local zones than on intervals with no zones.

4.2 Illustrative examples of flow conditions in deposition drifts

To visualize the flow conditions in the deposition drifts, two realizations of the possible flow conditions along the deposition drifts were made and are presented in Figures 4-2 and 4-3. For the realizations, simulations with the Fracman software /Dershowitz et al. 1994/ with tentative fracture parameters were done. In the future studies, more attention should be paid in correcting the orientation bias. Also the size distribution of the fractures should be estimated more thoroughly; here the size distribution presented in /Hellä et al. 2004b/ was used.

To visualise the possible flow conditions along the deposition drifts two realizations were created based on the analysis result. Fracture zones were assumed to occur one per 150 m drift length. To overcome the difficulty to apply the data from the subvertical boreholes to horizontal deposition drifts quick simulations with the Fracman software were done. The purpose was mainly to get an idea how the introduction of vertical features would effect the possible number of intersections between transmissive fractures (outside the zones) and horizontal drifts. Three fracture sets with different orientation were assumed to exist. The mean orientation of the sets is estimated visually from the Figure 3-8. The dispersion of the horizontal set is given a value that allows large variation around the mean orientation and for the vertical sets only little variation around the mean is given. The P_{32} values were adjusted to give a reasonable match with the observed borehole intersections. The parameters used are shown in Table 4-2. It is pointed out that these parameters are very tentative and not based on a thorough analysis, which was not in scope of this work. Especially the distribution parameters of the Fisher distribution are hardly more than guesses. The size distribution parameters on the hand are based on the data of estimated size of the larger hydraulic features in the near surface part of the rock (0 to –300 m). The original data used for size analysis is as such uncertain and as it describes larger scale features it is not very suitable to estimate the size of the single transmissive fractures.

Table 4-2. Parameters used in the simulations.

	Intensity P_{32} (fracture area per volume)	Mean orientation (dip direction/dip)	Orientation distribution	Size Power law distribution
Set 1	0.0192	160°/20°	Fisher(3)	X_{min}=20, shape factor, b=1.6
Set 2	0.0068	320°/80°	Fisher(50)	X_{min}=20, b=1.6
Set 3	0.0049	90°/90°	Fisher(50)	X_{min}=20, b=1.6

According to the simulation the number of intersections between the deposition drift and the each of the fracture sets varied from 0–3. This result was used together with the distribution of the transmissivity, the frequency of the transmissive fractures and their mutual distance to put up examples of possible flow conditions along the drifts. Figures 4-2 and 4-3 present the realizations of the transmissive fractures and drift inflow along a deposition drift. Figures 4-4 and 4-5 show the transmissivity distribution and the distribution of the distance between transmissive fractures in the two realizations compared to observed ones. In one of the realizations (Drift 1) a narrow, local zone is included, as according to available borehole data such local zones occur with the frequency of approximately one per 150 m, whereas Drift 2 contains no zones.

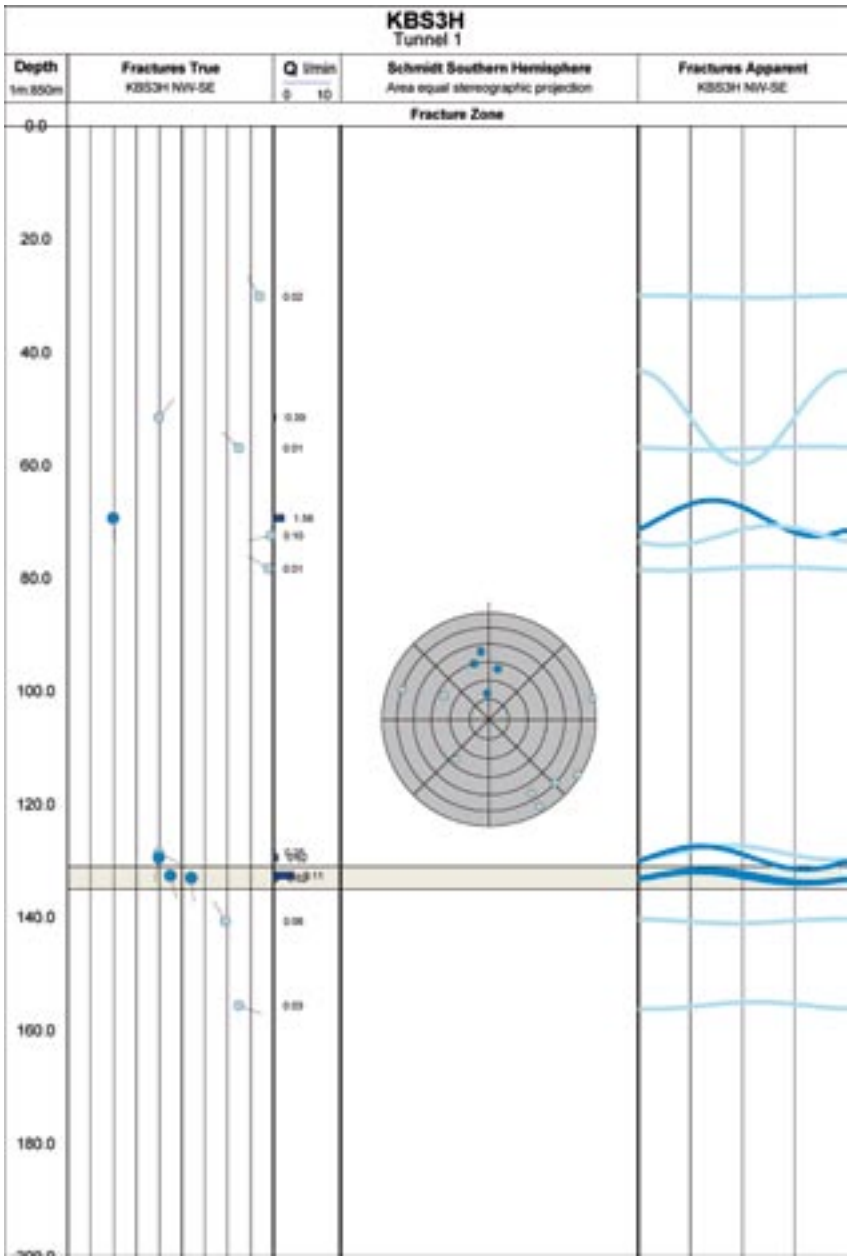

Figure 4-2. *Example of possible flow conditions in a 200 m deposition drift – Drift 1.*

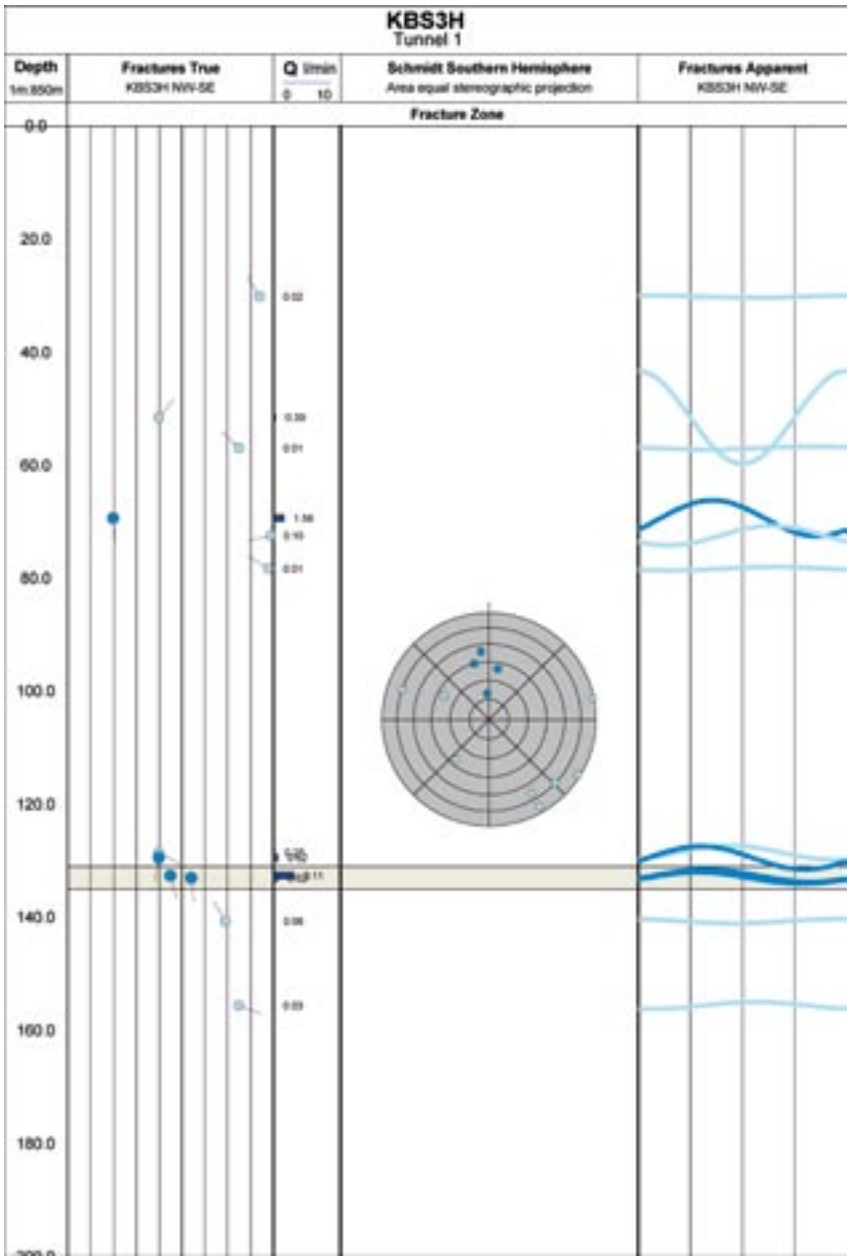

Figure 4-3. *Example of possible flow conditions in a 200 m deposition drift – Drift 2.*

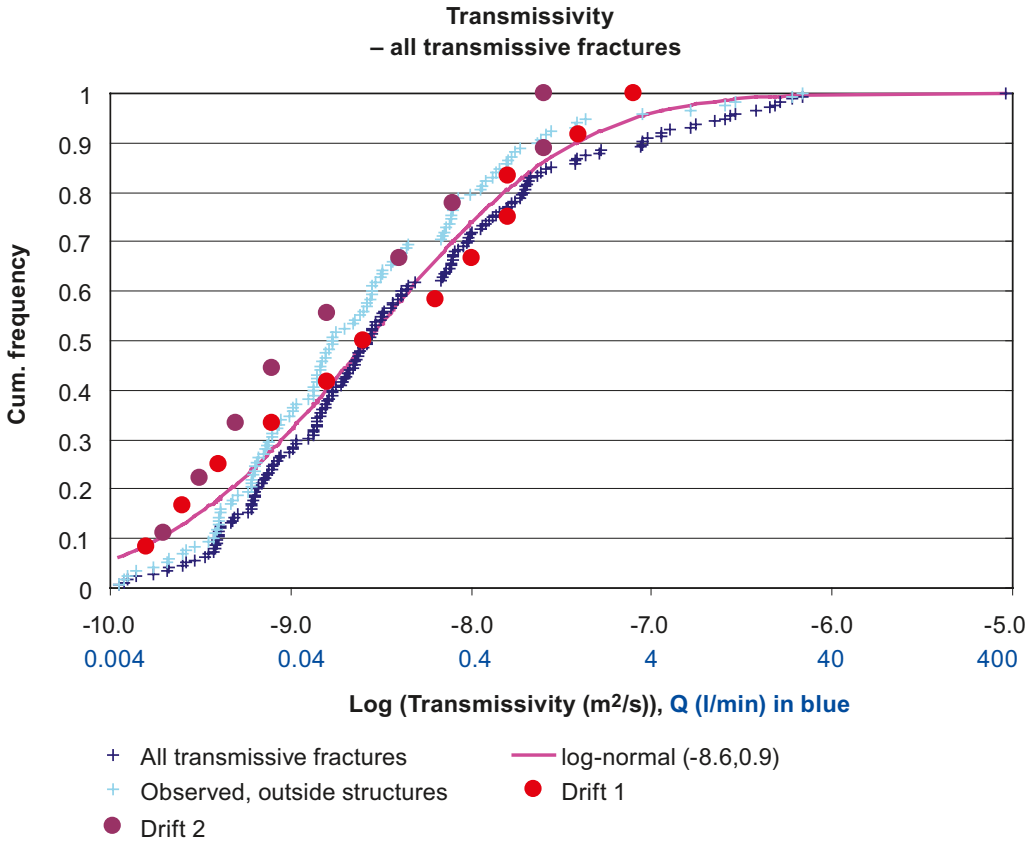

Figure 4-4. *Transmissivity (log(T, m^2/s)) distribution in the two realizations compared to observed one. Drift 1 contains one narrow, local zone, Drift 2 no such zone.*

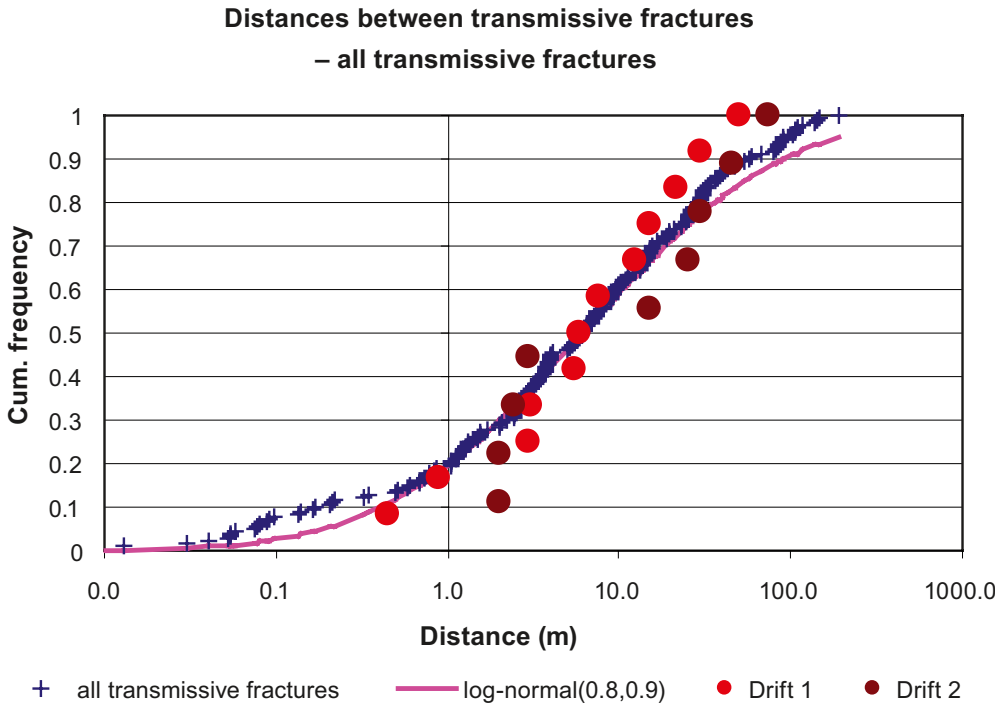

Figure 4-5. *Distribution of the distance between transmissive fractures in the two realizations compared to the observed one.*

5 Discussion

The study is based on the observations of transmissive fractures in the boreholes. The major fracture zones and the surrounding rock have been excluded as the aim has been to analyze likely conditions in the deposition drifts. The transmissivity of the fractures ranges from 10^{-10} m^2/s to 10^{-5} m^2/s corresponding to drift inflow of 0.004 l/min and 400 l/min respectively. The overall frequency of transmissive fractures is 4 fractures per 100 m, when considering all the fractures with measured flow. The transmissive fractures at the studied depth range occur mainly in connection of local zones or abundant fracturing. This is true especially for the fractures with transmissivity higher than $T > 10^{-8}$ m^2/s (flow greater than 0.4 l/min). Fractures with smaller transmissivity occur also outside the zones, but also then they tend to form clusters. Intervals over 100 m with no transmissive fractures form about one fifth of the total sample length included in the study and intervals with no highly transmissive fractures ($T > 10^{-8}$ m^2/s) cover roughly 80% of the sample length. The transmissivity of fractures per 5 m and per 10 m borehole length were summarised and converted to drift inflow. Over 90% of the 5 m intervals and about 85% of the 10 m intervals had an equivalent drift inflow less than 0.1 l/min. There would be likely two 5 m and one or two 10 m intervals per 100 m drift length with inflows higher than 0.1 l/min, which agrees with the frequency of such features keeping in mind the clustering of the transmissive fractures.

The occurrence of local zones is assumed to be about 1 per 150 m i.e. approximately 1–3 per 300 m drift. The majority of the observed zones have a sub-horizontal to intermediate dip towards southeast. The fracture and crushed zones are rather narrow with a mean thickness for fracture zones being 6.1 m and for crushed zones 8.9 m /Vaittinen et al. 2003/. These figures include all fracture borehole interval regardless of the depth and also the intersection with major zones defined in chapter 2.4. The local zones considered here have mainly thickness of few meters. Therefore in case the zones are intersected perpendicularly, the intersection of a fracture zone with the drift is likely to have a length of the same order as the combined supercontainer and distance block length i.e. taking a total length of about 10 to 30 m i.e. up to 10% of the deposition drift length (300 m). Naturally, the length of the intersection of the zone with the drift can be much higher in case of gentle intersection angle. Also, it should be remembered that the boreholes have a considerably smaller diameter than the deposition drift. As a consequence, the length of the zone intersection with the drift is larger than with the borehole even if the intersection deviates only slightly from the perpendicular.

There are significant uncertainties in applying the presented results based on the observations from mainly subvertical boreholes to horizontal drifts due to the orientation bias. Majority of the observed transmissive fractures and the local zones have a gentle dip towards southeast. Such features would intersect the horizontal with a gentle angle meaning a rather long intersection length. On the other hand, the intersection probability is rather low. The boreholes detect poorly vertical fractures practically in any direction, features, which in turn are the ones with the highest intersection probability with the horizontal drifts if having an appropriate strike. In the further analysis it is possible to correct the orientation bias using e.g. /Terzaghi 1965/ correction. Still, there is hardly any information available on the size of the transmissive fractures.

It is questionable whether the hydraulic properties are isotropic and the results obtained from the mainly subvertical boreholes can be extended to horizontal deposition drifts of the KBS-3H alternative. As a matter of fact, there is strong evidence of anisotropic nature of the Olkiluoto bedrock (e.g. foliation). Estimation of the inflow to the deposition drift based on the observed transmissivity in boreholes assuming steady state radial flow includes also several limitations. The heterogeneity e.g. channelling of the flow within the fractures or connectivity between hydraulic features is not taken into account. The eventual inflows to the deposition drift will be affected by grouting and skin effects around the drift, which are both likely to limit the flow into the drift.

6 References

ALT 2001. WellCAD user's guide for version 3.0. Advanced Logic Technologies, Luxembourg. 831 p.

Dershowitz W, Lee G, Geier J, Hitchcock S, LaPointe P, 1994. Fracman Interactive discrete feature data analysis, geometric modelling, and exploration simulation. User Documentation Version 2.4. Seattle, USA: Golder Associates Inc. 172 s. + app.

Gardemeister R, Johansson S, Korhonen P, Patrikainen P, Tuisku T, Vähäsarja P, 1976. The application of Finnish engineering geological bedrock classification (in Finnish). Espoo, Finland: Technical Research Centre of Finland, Geotechnical laboratory. 38 p. Research note 25.

Hämäläinen H, 1991a. Hydraulical Testing at Olkiluoto, Borehole KR1 (in Finnish with an English abstract). Helsinki, Finland: Teollisuuden Voima Oy. TVO/Site investigations Work Report 91-04.

Hämäläinen H, 1991b. Hydraulical Testing at Olkiluoto, Boreholes KR2, KR3, KR4 and KR5 (in Finnish with an English abstract). Helsinki, Finland: Teollisuuden Voima Oy. TVO/Site investigations Work Report 91-05.

Hämäläinen H, 1997a. Measurements of hydraulic conductivity at Olkiluoto in Eurajoki, borehole OL-KR1. Working Report 97-03. Posiva Oy, Helsinki. 476 p. (Vol 1 and 2) (in Finnish).

Hämäläinen H, 1997b. Measurements of hydraulic conductivity at Olkiluoto in Eurajoki, borehole OL-KR2. Working Report 97-21. Posiva Oy, Helsinki. 820 p. (Vol 1 and 2) (in Finnish).

Hämäläinen H, 1997c. Measurements of hydraulic conductivity at Olkiluoto in Eurajoki, borehole OL-KR4. Working Report 97-45. Posiva Oy, Helsinki. 1079 p. (Vol 1, 2 and 3) (in Finnish).

Hämäläinen H, 1997d. Measurements of hydraulic conductivity at Olkiluoto in Eurajoki, borehole OL-KR8. Working Report 97-46. Posiva Oy, Helsinki. 333 p (in Finnish).

Hämäläinen H, 1997e. Measurements of hydraulic conductivity at Olkiluoto in Eurajoki, borehole OL-KR10. Working Report 97-47. Posiva Oy, Helsinki. 243 p (in Finnish).

Hellä P, Tammisto E, Ahokas H, 2004a. Hydraulically conductive fractures and their properties in boreholes KR4 and KR7–KR10 at Olkiluoto site. Olkiluoto, Finland: Posiva Oy. 84 p. Working report 2004-21.

Hellä P, Vaittinen T, Saksa P, Nummela J, 2004b. Statistical Analysis and Modelling of Olkiluoto Structures. Eurajoki, Finland: Posiva Oy. 56 p. Working Report 2004-58.

Ikonen K, 2005. Thermal Condition of Open KBS-3H Tunnel. Olkiluoto, Finland: Posiva Oy. 34 p. POSIVA 2005-04.

Korhonen K-H, Gardemeister R, Jääskeläinen H, Niini H, Vähäsarja P, 1974. Engineering geological bedrock classification (in Finnish). Espoo, Finland: Technical Research Centre of Finland, Geotechnical laboratory. 78 p. Research note 12.

La Pointe P, Hermanson J, 2002. Estimation of rock movements due to future earthquakes at four Finnish candidate repository sites. Helsinki, Finland: Posiva Oy. 89 p. Posiva-2002-02. ISBN 951-652-109-6.

Pöllänen J, Rouhiainen P, 1996a. Difference flow measurements at the Olkiluoto site in Eurajoki, boreholes KR1-KR4, KR7 and KR8. Helsinki: Posiva Oy. 44 p. Work Report PATU-96-43e.

Pöllänen J, Rouhiainen P, 1996b. Difference flow measurements at the Olkiluoto site in Eurajoki, boreholes KR9 and KR10. Helsinki, Finland: Posiva Oy. Work report PATU-96-44e

Pöllänen J, Rouhiainen P, 2000. Difference flow measurements at the Olkiluoto site in Eurajoki, borehole KR11. Working Report 2000-38. Posiva Oy, Helsinki.

Pöllänen J, Rouhiainen P, 2001a. Difference flow and electric conductivity measurements at the Olkiluoto site in Eurajoki, boreholes KR6, KR7 and KR12. Working Report 2000-51. Posiva Oy, Helsinki. 150 p.

Pöllänen J, Rouhiainen P, 2002a. Difference flow and electric conductivity measurements at the Olkiluoto site in Eurajoki, boreholes KR13 and KR14. Working Report 2001-42. Posiva Oy, Helsinki. 100 p.

Pöllänen J, Rouhiainen P, 2002b. Flow and electric conductivity measurements during long-term pumping of borehole KR6 at the Olkiluoto site in Eurajoki. Helsinki, Finland: Posiva Oy, 67 p. Working Report 2001-43.

Pöllänen J, Rouhiainen P, 2002c. Difference flow and electric conductivity measurements at the Olkiluoto site in Eurajoki, boreholes KR15-KR18 and KR15B-KR18B. Helsinki, Finland: Posiva Oy. 134 p. Working Report 2002-29.

Pöllänen J, Rouhiainen P, 2002d. Difference flow measurements at chosen depths in boreholes KR1, KR2, KR4 and KR11 at the Olkiluoto site in Eurajoki. Helsinki, Finland: Posiva Oy. 31 p. Working Report 2002-42.

Poteri A, 2001. Estimation of the orientation distributions for fractures at Hästholmen, Kivetty, Olkiluoto and Romuvaara. Helsinki, Finland: Posiva Oy. 18 p. Working report 2001-10.

Rautakorpi J, Johansson E, Tinucci J, Palmén J, Hellä P, Ahokas H, Heikkinen E, 2003. Effect of fracturing on tunnel orientation using KBTunnel and 3DEC programmes for the repository of spent nuclear fuel at Olkiluoto. Olkiluoto, Finland: Posiva Oy. 38 p. Working report 2003-09.

Rouhiainen P, 2000. Electrical conductivity and detailed flow logging at the Olkiluoto site in Eurajoki, boreholes KR1-KR11. Working Report 99-72. Posiva Oy, Helsinki.

Terzaghi R D, 1965. Sources of Error in Joint Surveys. Geotechnique 15, 287 – 304.

Vaittinen T, Ahokas H, Heikkinen E, Hellä P, Nummela J, Saksa P, Tammisto E, Paulamäki S, Paananen M, Front K, Kärki A, 2003. Bedrock model of the Olkiluoto site, version 2003/1. Olkiluoto, Finland: Posiva Oy. 266 p. Working report 2003-43.

Öhberg A, Rouhiainen P, 2000. Posiva Groundwater Flow Measuring Techniques. Helsinki, Finland: Posiva Oy. 81 p. Posiva-2000-12. ISBN 951-652-098-7.